Pergamon

Int. J. Solids Structures Vol. 33, No. 15, pp. 2133–2159, 1996

0020–7683/96 $15.00 + .00

0020–7683(95)00139–5

INFLUENCE OF CONTINUITY AND ASPECT-RATIO ON THE BUCKLING OF SKEW PLATES AND PLATE ASSEMBLIES

C. B. YORK†
Department of Civil and Environmental Engineering, The University of Edinburgh, Crew Building, The King's Buildings, Edinburgh EH9 3JN, U.K.

(*Received* 15 *February* 1995)

Abstract—New buckling interaction results are presented for skew plates and prismatic assemblies of plates, which illustrate the influence of continuity over supports for a range of aspect-ratio and loading combinations. The work follows from initial comparisons (York and Williams, 1995, Buckling analysis of skew plate assemblies: classical plate theory results incorporating Lagrangian multipliers. *Comput. Struct.* **56**, 625–635) with those in the literature for *isolated* plates and stiffened benchmark panels, consisting of prismatic assemblies of plates.

The analysis method, which is an enhancement to the existing computer program VICONOPT, is based on an "exact" analytical solution using Classical Plate Theory. This accounts for an infinitely long prismatic plate assembly supported at regular intervals over supports with general skew angle α, forming a series of skew plates or plate assemblies joined end to end. This modelling can be described as exhibiting *uni-axial continuity*. The enhancement relates to a recent modification of the recurrence equations, which now accounts for infinitely wide skew plate assemblies supported at regular transverse intervals. This modelling possesses *bi-axial continuity*. Crown copyright © 1996 Published by Elsevier Science Ltd.

1. INTRODUCTION

There now exists a significant number of published buckling results dealing with in-plane compression or shear loaded skew plates, which date back to the early 1950s, when post-war investigations began to reveal the potential of using skew plates in the then new swept-wing aircraft concept. They cover a host of boundary conditions ranging from simply supported on all four edges (Durvasula, 1971; Fried and Schmitt, 1972; Kennedy and Prabhakara, 1978/79; Mizusawa *et al.*, 1980; Thangam Babu and Reddy, 1978; Wang *et al.*, 1992; Wittrick, 1956), through to clamped on all four edges (Argyris, 1966; Durvasula, 1970; Fried and Schmitt, 1972; Guest, 1951; Prabhu and Durvasula, 1972; Wittrick, 1953/4), some of which illustrate the effects of combining clamped, simply supported and free edges. With few exceptions however, all previous work on skew plates deal with the isolated plate, i.e. a plate of finite length and finite width, which does not account for the effect of continuity over supporting edges. Mizusawa and Kajita (1986) included rotational edge stiffnesses, which may account for the effects of continuity, though the problem of obtaining correct values for such stiffnesses must first be resolved.

Three categories are now defined that classify the various forms of plate continuity over their supporting edges, which are then used throughout the study that follows. They are defined as: (1) isolated, i.e. of finite length and finite width; (2) exhibiting uni-axial continuity, i.e. continuous over supports along a single axis; and (3) exhibiting bi-axial continuity. Examples are given in the next paragraph.

Results were presented by York and Williams (1995) which fall into the second category. These were for infinitely long prismatic plates and plate assemblies, which were supported at regular longitudinal intervals, producing continuity of the plate (over supports) along a single axis. Comparison was made with isolated, compression loaded skew plate results in the literature, which had all four edges either simply supported or clamped. The clamped results agreed favourably since, by implication, they degenerate into isolated

†Formerly at the Division of Structural Engineering, Cardiff School of Engineering, Queens Buildings, University of Wales Cardiff, PO Box 917, Cardiff CF2 1XH, U.K.

plates. For the simply supported case however, previous results gave significant disagreements with each other, hence definitive conclusions were difficult to draw other than that upper-bounds were obtained when $\alpha > 0°$. This was expected, because the physical problem solved was different. Additionally, buckling results were presented for four well known panel benchmarks to illustrate the effect that shear loading can have on the stability of longitudinally compressed stiffened skew panels, as well as highlighting the implications of designing such panels as if they were rectangular in plan, which can lead to significant errors on the unsafe side. It is believed that these category (2) results go some way to being a true representation of aircraft wing panel construction. The characteristic which makes this representation complete is the concept adopted by Anderson (1951), who gave results for the third category, whereby a flat sheet, extending to infinity in all directions, was subdivided by a series of equally-spaced non-deflecting supports into an array of identical oblique (skew) plates to which compressive stresses were applied both parallel and perpendicular to one support direction. The energy method was used with certain simplifying assumptions for the deflection pattern across the array. In the corresponding problem for an array of rectangular plates, the nodal lines of the buckled deflection pattern are straight and parallel to the supporting sides, hence adjacent plates buckle identically but in opposite directions, the boundary conditions for an individual plate are therefore those of simple supports. The problem for the oblique case has been described by Wittrick (1953) and Morley (1963) as similar to that of an array of rectangular plates in shear, whereby the buckling pattern repeats over a certain number of plates in both directions and that any nodal lines which may occur are straight but not necessarily parallel to the supports.

It is the concept of bi-axial continuity, along both longitudinal and transverse axes, that forms the subject of the current paper. A summary of the main theoretical aspects of the analysis, which span several published papers, is developed in the following section. Thereafter, results are given, which demonstrate the effect that continuity over supports has on the buckling characteristics of both skewed stiffened panels and plates.

2. FORMULATION

The analysis method (Wittrick and Williams, 1974; Williams and Anderson, 1983) is based on the Kirchoff-Love hypothesis. The general form of the differential equation of equilibrium is given by

$$D_{11}\frac{\partial^4 w}{\partial x^4}+4D_{16}\frac{\partial^4 w}{\partial x^3\,\partial y}+2(D_{12}+2D_{66})\frac{\partial^4 w}{\partial x^2\,\partial y^2}+4D_{26}\frac{\partial^4 w}{\partial x\,\partial y^3}+D_{22}\frac{\partial^4 w}{\partial y^4}$$
$$+N_x\frac{\partial^2 w}{\partial x^2}+2N_{xy}\frac{\partial^2 w}{\partial x\,\partial y}+N_y\frac{\partial^2 w}{\partial y^2}=0 \quad (1)$$

and the stress-strain relationship for each lamina is given by

$$\begin{Bmatrix}\sigma_x\\ \sigma_y\\ \tau_{xy}\end{Bmatrix}=\begin{bmatrix}\bar{Q}_{11} & & \text{Sym}\\ \bar{Q}_{12} & \bar{Q}_{22} & \\ \bar{Q}_{16} & \bar{Q}_{26} & \bar{Q}_{66}\end{bmatrix}\begin{Bmatrix}\varepsilon_x\\ \varepsilon_y\\ \gamma_{xy}\end{Bmatrix} \quad (2)$$

where the $\bar{Q}_{ij}$ represent the transformed reduced stiffnesses, the relationships for which are derived and defined by Jones (1975).

Classical Lamination Theory (CLT) is assumed in obtaining composite panel results, hence orthotropic layers are assumed to be perfectly bonded together with a non-shear-deformable infinitely thin bond-line. The solution permits orthotropic in-plane material properties (so that $A_{16} = A_{26} = 0$) and uncoupled anisotropic out-of-plane (i.e. flexural) properties, so that $\underset{\sim}{\mathbf{B}} = \underset{\sim}{0}$. Balanced and symmetric laminates eliminate shear- and bending-extension coupling respectively.

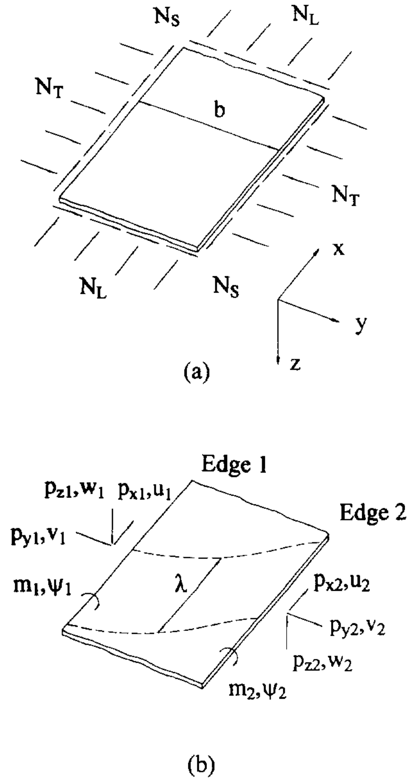

Fig. 1. (a) Loading and reference axis system for a component plate of width b; and (b) skew mode with half-wavelength λ and the perturbation force (denoted by p and m) and displacement amplitudes at the longitudinal edges of the plate, which are multiplied by $\exp(i\pi x/\lambda)$.

Figure 1(a) shows a component plate of width b, together with the basic longitudinally invariant in-plane forces which are carried. These are forces of N_L, N_T and N_S per unit length, corresponding to uniform longitudinal and transverse compressive forces and shear flow, respectively. The deflections of the plate assembly are assumed to vary sinusoidally in the longitudinal direction with half-wavelength λ. The nodal lines of the deflection pattern, shown dashed on Fig. 1(b), are perpendicular to the longitudinal direction when all the plates of a plate assembly are isotropic or orthotropic and are subject only to N_L and/or N_T. The nodal lines are then consistent with transverse simple supports at the ends of each plate of the assembly, and so exact results are obtained for such end conditions if λ is taken as $\lambda_j = a/j$, where the integer $j = 1, 2, 3\ldots$ and a is the length of the assembly. Skewed nodal lines result when some of the component plates are anisotropic or carry in-plane shear loads N_S. They are inconsistent with transverse simple supports and so form only approximate solutions for such supports. This approximation however, is overcome by the method of Lagrangian multipliers, which is described below.

Displacements at nodes, i.e. junctions between the longitudinal plates, are given by the real part of $\underset{\sim}{\mathbf{D}}'_j\exp(i\pi x/\lambda_j)$, where $i = \sqrt{-1}$, x is the longitudinal co-ordinate and $\underset{\sim}{\mathbf{D}}'_j$ contains the four complex displacement amplitudes for each node which correspond, in order, to the ψ, w, v and u of Fig. 1(a). All possible types of mode are included by permitting the junctions between individual plates to flex (Wittrick and Williams, 1974). Critical loads are the eigenvalues corresponding to $\underset{\sim}{\mathbf{K}}_j\underset{\sim}{\mathbf{D}}_j = \underset{\sim}{0}$, where $\underset{\sim}{\mathbf{D}}_j$ is obtained by multiplying every fourth element of $\underset{\sim}{\mathbf{D}}'_j$, associated with longitudinal displacement, by i. This i takes account of a 90° spatial phase difference between these displacements and others which occur for plate assemblies consisting of orthotropic plates with no shear loading, i.e. $N_s = 0$.

Note that $\underset{\sim}{\mathbf{K}}_j$ is a transcendental function of λ and load factor, which changes from being complex and Hermitian to being real and symmetric when all component plates are isotropic or orthotropic and $N_S = 0$. Due to this transcendental nature, usual linear eigenvalue methods are inapplicable. However for such exact stiffness matrix analysis the general Wittrick-Williams algorithm (Wittrick and Williams, 1973) removes the possibility of eigenvalues ever being missed despite the transcendental nature of the problem. Therefore this algorithm was used to ensure that for any value of λ_j, the lowest critical buckling load is not confused with higher ones.

For skew plate assemblies, the prismatic nature of the plate assembly must be maintained since arbitrarily orientated stiffeners can not be accounted for. Instead, point supports are used to produce the (skew) transverse boundaries. They are enforced by the method of Lagrangian multipliers, which was already present in the theory because it was needed to overcome the problem associated with shear loaded rectangular plates (Anderson *et al.*, 1983). Each point support may constrain any combination of the four displacement amplitudes ψ, w, v and u. They may also constrain rotation ψ_y (ψ_z) about the y-axis (z-axis) to impose clamped conditions. This is obtained by differentiating the displacement function in the z (y) direction, e.g. $-i\pi w/\lambda$ replaces the displacement amplitude for rotation about the y-axis since

$$-\frac{\partial}{\partial x}(w\cdot e^{i\pi x/\lambda}) = -(i\pi/\lambda)w\cdot e^{i\pi x/\lambda}. \tag{3}$$

To include such point supports the fundamental equations become:

$$\left.\begin{aligned} &a\underset{\sim}{\mathbf{K}}_m\underset{\sim}{\mathbf{D}}_m+\underset{\sim}{\mathbf{e}}_m^H\underset{\sim}{\gamma}_n = \underset{\sim}{0} \quad (m = n+qM, \quad q = 0,\pm 1,\pm 2,\ldots) \\ &\sum\underset{\sim}{\mathbf{e}}_m\underset{\sim}{\mathbf{D}}_m = \underset{\sim}{0} \end{aligned}\right\} \tag{4}$$

where H denotes Hermitian transpose and it is sufficient here to note that $\underset{\sim}{\gamma}$ and $\underset{\sim}{\mathbf{e}}$ are the Lagrangian multiplier vectors and constraint matrices defined later in eqns (10) and (11) respectively, while $\underset{\sim}{\mathbf{K}}_m$ and $\underset{\sim}{\mathbf{D}}_m$ are defined beneath eqn (7). The equations apply to any infinitely long plate assembly which repeats at longitudinal intervals, to form identical bays of length a. The mode is assumed to repeat over M bays, i.e. over a length $L = Ma$. All modes can be obtained by simultaneously satisfying these equations in turn for each of the integers n given by

$$-M'' \leqslant n \leqslant M' \tag{5}$$

where M'' and M' are, respectively, the integer parts of $(M-1)/2$ and $M/2$. A complete solution is obtained by repeating the computations which follow at sufficient values of M. For the values of M chosen, the analysis assumes that the nodal displacements and forces of the plate assembly can be expressed, respectively, as the Fourier series:

$$\underset{\sim}{\mathbf{D}}_A = \sum_{m=-\infty}^{\infty}\underset{\sim}{\mathbf{D}}_m\exp\left(\frac{2i\pi mx}{L}\right) \tag{6}$$

$$\underset{\sim}{\mathbf{P}}_A = \sum_{m=-\infty}^{\infty}\underset{\sim}{\mathbf{K}}_m\underset{\sim}{\mathbf{D}}_m\exp\left(\frac{2i\pi mx}{L}\right) \tag{7}$$

where $\underset{\sim}{\mathbf{D}}_m$ and $\underset{\sim}{\mathbf{K}}_m$ are the $\underset{\sim}{\mathbf{D}}_j$ and $\underset{\sim}{\mathbf{K}}_j$ defined above, for $\lambda = \lambda_m$, where $\lambda_m = L/2m$ and $m = 1, 2, 3,\ldots$ The total energy of a length L of the plate is expressed in terms of the stiffness matrices $\underset{\sim}{\mathbf{K}}_m$.

The governing equations are now obtained by the method of Lagrangian multipliers, by which the total energy is minimised subject to the constraints needed to represent the point attachments of the plate assembly to the rigid point supports. Equation (8) follows, which is similar in form to eqns (4) written as a single equation.

$$\begin{bmatrix} L\mathbf{K}_0 & & & & & \mathbf{E}_0^T \\ & L\mathbf{K}_1 & & & & \mathbf{E}_1^H \\ & & L\mathbf{K}_{-1} & & & \mathbf{E}_{-1}^H \\ & & & L\mathbf{K}_2 & & \mathbf{E}_2^H \\ & & & & L\mathbf{K}_{-2} & \mathbf{E}_{-2}^H \\ & & & & \ddots & \vdots \\ \mathbf{E}_0 & \mathbf{E}_1 & \mathbf{E}_{-1} & \mathbf{E}_2 & \mathbf{E}_{-2} \quad \cdots & \mathbf{0} \end{bmatrix} \begin{Bmatrix} \mathbf{D}_0 \\ \mathbf{D}_1 \\ \mathbf{D}_{-1} \\ \mathbf{D}_2 \\ \mathbf{D}_{-2} \\ \vdots \\ \mathbf{P}_L \end{Bmatrix} = \mathbf{0} \tag{8}$$

where negative signs indicate complex conjugates. This is valid for any prismatic plate assembly with responses which repeat over length Ma. The Lagrangian multipliers repeat over this length such that

$$\mathbf{P}_L^T = [\mathbf{P}_{L0}^T, \mathbf{P}_{L1}^T, \mathbf{P}_{L2}^T, \ldots] \tag{9}$$

with $\mathbf{P}_{Lk}^T = \mathbf{P}_{L,k+M}^T$ representing the Lagrangian multipliers in the interval $ka \leqslant x < (k+1)a$. The above equation is satisfied by the complex Fourier series

$$\mathbf{P}_{Lk} = \sum_{j=-M''}^{M'} \boldsymbol{\gamma}_j \exp\left(\frac{2i\pi jk}{M}\right) \tag{10}$$

The constraint matrix $\mathbf{E}_m$ can be expressed as

$$\mathbf{E}_m^T = [\mathbf{e}_m^T, \mathbf{e}_{m1}^T, \mathbf{e}_{m2}^T, \ldots] \tag{11}$$

where $\mathbf{e}_{mk}$ is the constraint matrix for bay $ka \leqslant x < (k+1)a$.

The solution given by the above includes all modes with wavelength L, $L/2$, $L/3$, etc. However, by decoupling the equations and selecting m numbers that produce repetition over Ma and not also over some fraction of Ma, greater efficiency is achieved by avoiding computation involving values of m not contributing to the solution. Hence, because $\lambda_m = L/2m$ and $L = Ma$, the values of m previously defined in eqns (4) give:

$$\lambda_m = a/\{(2n/M)+2q\} \quad q = 0, \pm 1, \pm 2, \ldots \tag{12}$$

From eqn (12), the λ_ms are functions of M/n and not of M and n independently. Therefore computational savings are made by only considering combinations of M and n which do not share the same value of M/n. It is convenient here to express the resulting relationships in terms of the single parameter $\xi = 2n/M$, so that eqn (12) can be rewritten as

$$\lambda_m = \frac{a}{(\xi+2q)} \quad q = 0, \pm 1, \pm 2, \ldots \tag{13}$$

Higher accuracy is achieved, at the expense of increased solution time, by increasing both q_{max}, the maximum value of q used in eqn (13), and also the number of ξ in the range $0 \leqslant \xi \leqslant 1$.

The theory presented above is incorporated in the existing 36,000 line, FORTRAN 77 computer program VICONOPT (VIPASA with CONstraints and OPTimisation) (Williams *et al.*, 1991).

Transverse repetition

Many plate assemblies exhibit repetitive cross-sections which can be analysed by assuming infinite width and writing suitable recurrence equations. A brief summary of a recent publication (York and Williams, 1994) dealing with an extension of this theory for skew plate analysis follows.

For skew plate assemblies, constraints must be included in these recurrence equations such that the continuity of the line of supports is maintained in adjacent bays. This is achieved by introducing a constant longitudinal shift (x') to support locations at the start of each successive transversely adjacent portion. The fundamental equations for the repeating portion become:

$$\left.\begin{aligned} &a\underset{\sim}{\mathbf{K}}_{m0}\underset{\sim}{\mathbf{D}}_{m0}+\underset{\sim}{\mathbf{e}}^{H}_{m0}\underset{\sim}{\gamma}_{n0}=\underset{\sim}{0} \quad (m=n+qM, \quad q=0,\pm 1,\pm 2,\ldots) \\ &\sum \underset{\sim}{\mathbf{e}}_{m0}\underset{\sim}{\mathbf{D}}_{m0}=\underset{\sim}{0} \end{aligned}\right\} \tag{14}$$

where

$$\underset{\sim}{\mathbf{K}}_{m0}=\underset{\sim}{\mathbf{K}}_{m11}+\underset{\sim}{\mathbf{K}}^{H}_{m12}\exp\{-\mathrm{i}(\phi-2\pi m x'/Ma)\}+\underset{\sim}{\mathbf{K}}_{m12}\exp\{\mathrm{i}(\phi-2\pi m x'/Ma)\}. \tag{15}$$

Equations (14) must be solved for the same combinations of M and n, or values of ξ, as for plate assemblies that are not transversely repetitive. However, now suitable values of ϕ must be used for each combination. When $\alpha = 0^\circ$, eqn (15) reduces to the previously defined form (Williams and Anderson, 1985)

$$\underset{\sim}{\mathbf{K}}_{m0}=\underset{\sim}{\mathbf{K}}_{m11}+\underset{\sim}{\mathbf{K}}^{H}_{m12}\exp(-\mathrm{i}\phi)+\underset{\sim}{\mathbf{K}}_{m12}\exp(\mathrm{i}\phi) \tag{16}$$

and the values of ϕ can reasonably be restricted to those which give modes which repeat across twice the width of the assembly, so that, if P is the number of repeating portions of width b within the assembly,

$$\phi = \pi g/P \quad g = -(P-1),\ldots,-1,0,1,\ldots,P, \tag{17}$$

and the transverse half-wavelength λ_T is

$$\lambda_T = Pb/g = \pi b/\phi. \tag{18}$$

Because $\alpha \neq 0^\circ$ is now the general case, $x' \neq 0$ in eqn (15) and so the mode repeats over twice the width Pb of the assembly except that it is now moved along the assembly by $2x'$, such that it is skewed by the angle α, where $x' = b \cdot \tan\alpha$. Hence λ_T is the component, perpendicular to the longitudinal axis, of a half-wavelength that is skewed by the angle α.

3. RESULTS AND DISCUSSION

Buckling results for a selection of stiffened panels are presented at the beginning of this section. They are taken from a study by Stroud *et al.* (1984), which presents buckling results for seven such panels, using a number of analytical procedures that include EAL (Engineering Analysis Language), STAGS (STructural Analysis of General Shells) and VIPASA (Vibration and Instability of Plate Assemblies with Shear and Anisotropy) computer codes and forms a comprehensive benchmark study that has subsequently been used by others (Anderson *et al.*, 1983; Bushnell, 1987; Peshkam and Dawe, 1989; York and Williams, 1994) to evaluate new procedures. Thereafter, results are given for unstiffened panels (or plates) for which comparisons are made with those in the literature.

Stiffened panels

Each panel has 6 equally spaced stiffeners, diaphragm ends, and is subjected to various combinations of longitudinal compression and shear. The results presented here are for a composite blade-stiffened panel (Ex. 1 in Stroud *et al.*, 1984), metal blade-stiffened panel (Ex. 2), composite hat-stiffened panel (Ex. 5) and a metal j-stiffened panel (Ex. 7).

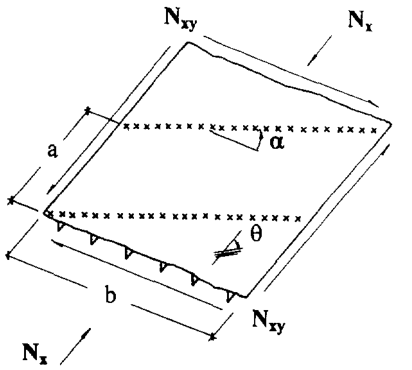

Fig. 2. Perspective showing typical arrangement for stiffened panel of width b, with continuity over skew supports at longitudinal intervals a. Directions of positive skew angle α, fibre orientation θ and shear (N_{xy}) and compression (N_x) loading are indicated.

The perspective of the blade-stiffened panel in Fig. 2 gives loading and dimensions which are common to the four panels. Note that the results for the panels maintain constant planform area for all skew angles α, i.e. the transverse (y) width $b = 762$mm and centre-line length $a = 762$mm are both constants. The simply supported boundary conditions at $y = 0$ and $y = b$ are $u = w = 0$, and at $x = 0$ and a they are $v = w = 0$.

The following four figures, Figs 3–6, give specific information regarding applied load, geometry and support location details for each panel. The cross-sections represent a repeating element which is equal to one sixth of the full panel width, hence for the two blade-stiffened panels (Ex. 1 and Ex. 2), the number of point supports on the panel is equal to 29. They prevent w displacement of the skin and v displacement of the stiffeners. At nodes which are common to both skin and stiffener, they prevent v and w. Tests confirmed (York, 1993; York and Williams, 1994) that these point support locations were sufficient to model

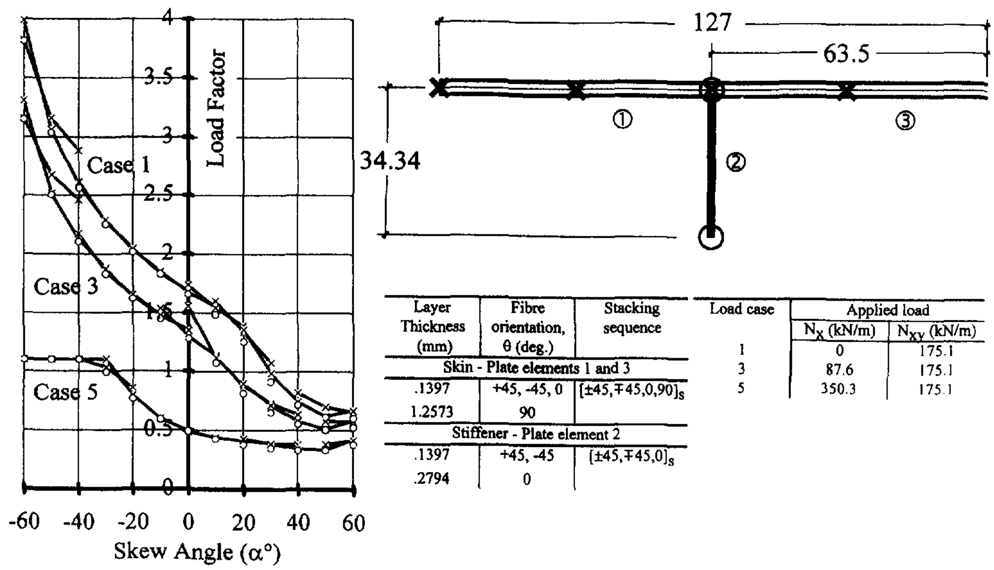

Layer Thickness (mm)	Fibre orientation, θ (deg.)	Stacking sequence
Skin - Plate elements 1 and 3		
.1397	+45, -45, 0	$[\pm45,\mp45,0,90]_s$
1.2573	90	
Stiffener - Plate element 2		
.1397	+45, -45	$[\pm45,\mp45,0]_s$
.2794	0	

Load case	Applied load	
	N_x (kN/m)	N_{xy} (kN/m)
1	0	175.1
3	87.6	175.1
5	350.3	175.1

Fig. 3. Category (3) buckling load factor results for the composite panel with 6 blade-stiffeners, corresponding to the three applied load cases given. Category (2) results are shown (○) for comparison. Layer thickness, fibre orientation and stacking sequence are given along with geometry, dimensions (in mm) and point support locations for a repeating portion of the panel. Supports ○, × or ⊗, which repeat at longitudinal intervals a, denote constraints of v, w, and v and w, respectively.

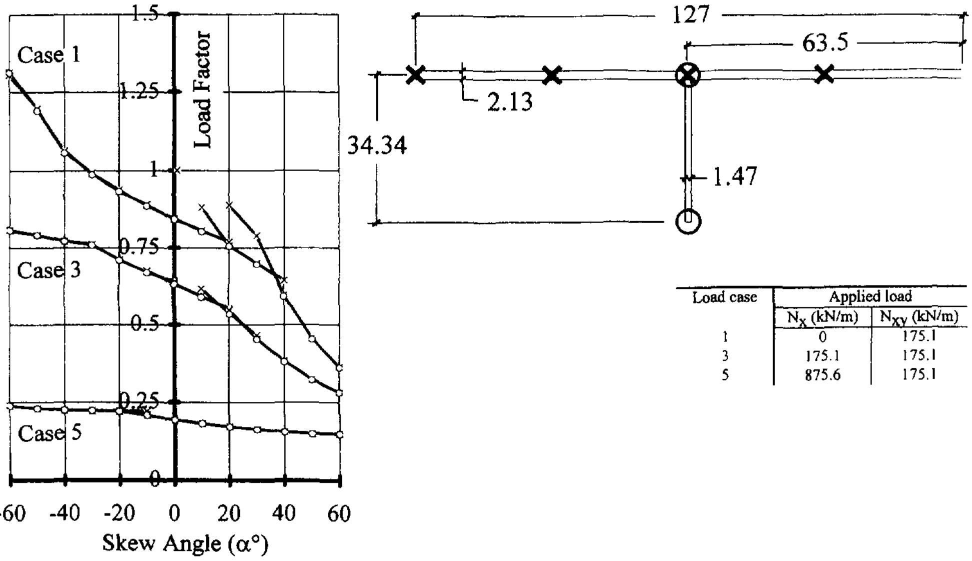

Load case	Applied load	
	N_X (kN/m)	N_{XY} (kN/m)
1	0	175.1
3	175.1	175.1
5	875.6	175.1

Fig. 4. Category (3) buckling load factor results for the metal panel with 6 blade-stiffeners, corresponding to the three applied load cases given. Category (2) results are shown (○) for comparison. Geometry, dimensions (in mm) and point support locations are illustrated for a repeating portion of the panel. Supports ○, × or ⊗, which repeat at longitudinal intervals a, denote constraints of v, w, and v and w, respectively.

a continuous line support for each skew angle and load combination. Buckling results for short wavelength modes were found to be insensitive to the number of point supports used in the model.

Each figure also presents buckling load factor curves for the bi-axially continuous stiffened panel subject to the combinations of shear (N_{xy}) and compression (N_x) loading

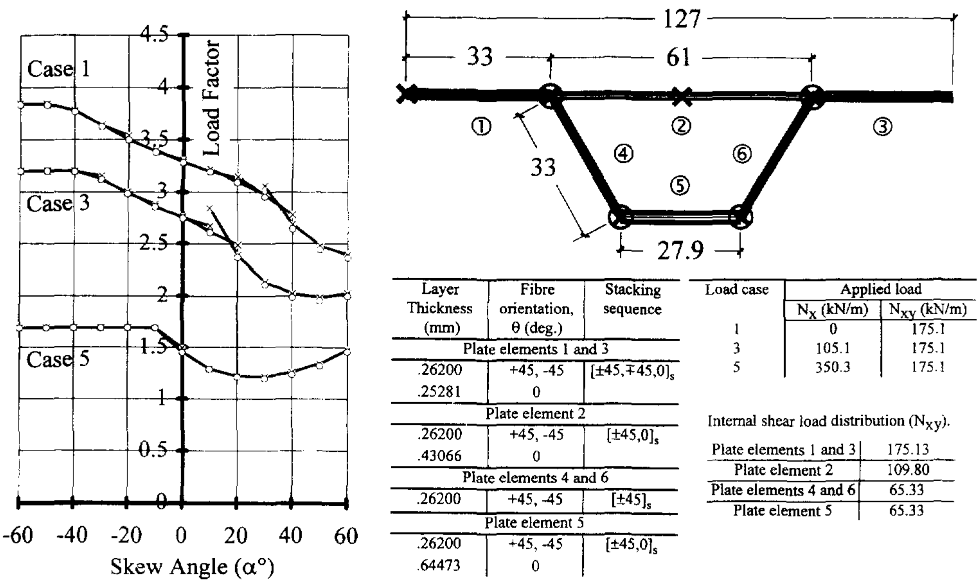

Layer Thickness (mm)	Fibre orientation, θ (deg.)	Stacking sequence
Plate elements 1 and 3		
.26200	+45, -45	$[\pm45,\mp45,0]_s$
.25281	0	
Plate element 2		
.26200	+45, -45	$[\pm45,0]_s$
.43066	0	
Plate elements 4 and 6		
.26200	+45, -45	$[\pm45]_s$
Plate element 5		
.26200	+45, -45	$[\pm45,0]_s$
.64473	0	

Load case	Applied load	
	N_X (kN/m)	N_{XY} (kN/m)
1	0	175.1
3	105.1	175.1
5	350.3	175.1

Internal shear load distribution (N_{XY}).

Plate elements 1 and 3	175.13
Plate element 2	109.80
Plate elements 4 and 6	65.33
Plate element 5	65.33

Fig. 5. Category (3) buckling load factor results for the composite panel with 6 hat-stiffeners, corresponding to the three applied load cases given. Category (2) results are shown (○) for comparison. Layer thickness, fibre orientation and stacking sequence are given along with geometry, dimensions (in mm) and point support locations for a repeating portion of the panel. Supports × and ⊗, which repeat at longitudinal intervals a, denote constraints of w, and v and w, respectively.

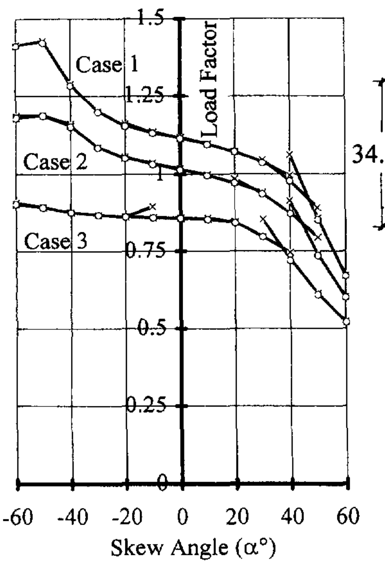

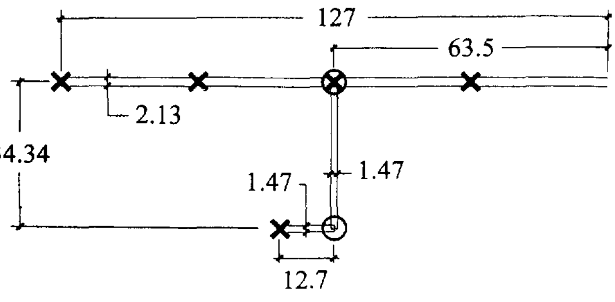

Load case	Applied load	
	N_x (kN/m)	N_{xy} (kN/m)
1	0	175.1
2	70.0	175.1
3	175.1	175.1

Fig. 6. Category (3) buckling load factor results for the metal panel with 6 j-stiffeners, corresponding to the three applied load cases given. Category (2) results are shown (○) for comparison. Geometry, dimensions (in mm) and point support locations are illustrated for a repeating portion of the panel. Supports ○, × or ⊗, which repeat at longitudinal intervals a, denote constraints of v, w, and v and w, respectively.

tabulated, where the buckling load is the product of load factor and applied load. To avoid congestion on the figures, only three of the six load cases presented by Stroud *et al.* (1984) are illustrated. Each envelope represents initial buckling for the load and skew angle (α°) combination. Cusps are indicated at changes in mode across the skew angle range, albeit with straight lines joining only the skew angles investigated. Discrete uni-axial results from York and Williams (1995) are indicated (○) for comparison. A comprehensive study of mode change across this skew angle range is detailed in York (1993). On all of the buckling diagrams presented, local modes cause a flattening of the curves over a range of skew angles.

The material properties for the two composite (blade- and hat-stiffened) panels are $E_1 = 131$ GPa, $E_2 = 13$ GPa, $G_{12} = 6.41$ GPa, $\nu_{12} = 0.38$ and $\nu_{21} = 0.0378$. The fibre orientations, layer thicknesses and stacking sequences for the skin and blades are also given in the figures. The positive fibre orientation angle θ is shown on Fig. 2. Material properties for the two metal panels are $E = 72.4$ GPa and $\nu = 0.32$.

The half-wavelengths (λ_m) coupled for calculation of all results in this paper, were obtained using $\xi = 0, 0.1, 0.2, \ldots\ldots, 0.9, 1$ and $q_{max} = 10$ and are listed in Table 1.

To obtain full accuracy agreement with results of the stiffened benchmark panels (Stroud *et al.*, 1984), positive shear loading is the reverse of that in Fig. 1, and is adopted only for the stiffened benchmark panels. Furthermore, consistency with the benchmark study was preserved by using units of imperial measure and ignoring the eccentric connections which are strictly required at stiffener/skin junctions.

Effects of continuity over supports for the rectangular ($\alpha = 0^\circ$) stiffened panels are displayed in Table 2 for the three categories. The most significant effect is demonstrated by comparison of the isolated panel with the panel which has longitudinal continuity over supports, i.e. categories (1) and (2) respectively. The rigorous finite element results of EAL and STAGS provide the isolated panel, category (1) comparisons. The results show further, the apparent insensitivity which exists for the same panels with added transverse continuity over supports, i.e. category (3) results. Table 3 demonstrates the percentage increase in shear buckling capacity that each of the four stiffened benchmark panels acquires from this added transverse continuity over supports for a range of skew angles. The composite blade-stiffened panel has clearly the highest increases, which is most likely due to the significant

Table 1. Half-wavelengths λ_m corresponding to the ξ values of eqn (13), used for all analyses ($q_{max} = 10$)

ξ	M	n	$m = n + qM$	$\lambda_m = Ma/2m$
0	1	0	$0; 1; 2; 3; \ldots$	$\infty; a/2; a/4; a/6; \ldots$
0.1	20	1	$1; 21, -19; 41, -39; 61, -59; \ldots$	$10a; 10a/21, -10a/19; 10a/41, -10a/39; 10a/61, -10a/59; \ldots$
0.2	10	1	$1; 11, -9; 21, -19; 31, -29; \ldots$	$5a; 5a/11, -5a/9; 5a/21, -5a/19; 5a/31, -5a/29; \ldots$
0.3	20	3	$3; 23, -17; 43, -37; 63, -57; \ldots$	$10a/3; 10a/23, -10a/17; 10a/43, -10a/37; 10a/63, -10a/57; \ldots$
0.4	5	1	$1; 6, -4; 11, -9; 16, -14; \ldots$	$5a/2; 5a/12, -5a/8; 5a/22, -5a/18; 5a/32, -5a/28; \ldots$
0.5	4	1	$1; 5, -3; 9, -7; 13, -11; \ldots$	$2a; 2a/5, -2a/3; 2a/9; -2a/7; 2a/13, -2a/11; \ldots$
0.6	10	3	$3; 13, -7; 23, -17; 33, -27; \ldots$	$5a/3; 5a/13, -5a/7; 5a/23, -5a/17; 5a/33, -5a/27; \ldots$
0.7	20	7	$7; 27, -13; 47, -33; 67, -53; \ldots$	$10a/7; 10a/27, -10a/13; 10a/47, -10a/33; 10a/67, -10a/53; \ldots$
0.8	5	2	$2; 7, -3; 12, -8; 17, -13; \ldots$	$5a/4; 5a/14, -5a/6; 5a/24, -5a/16; 5a/34, -5a/26; \ldots$
0.9	20	9	$9; 29, -11; 49, -31; 69, -51; \ldots$	$10a/9; 10a/29, -10a/11; 10a/49, -10a/31; 10a/69, -10a/51; \ldots$
1	2	1	$1; 3; 5; 7; \ldots$	$a; a/3; a/5; a/7; \ldots$

amount of 90° fibre that will account for added rotational stiffness when the panel is continuous transversely. This is also visible from the orthotropic "smeared" stiffnesses given for each panel in Table 2.

Plates

The plate results which follow, maintain a constant side- or aspect-ratio (a/b) as is usually adopted by others in the literature, hence unlike the stiffened panel results the planform area now changes with skew angle α.

York and Williams (1995) presented preliminary ($a/b = 1$) clamped plate results which were shown to agree favourably with others in the literature. A comprehensive study has since been made and is included here for completeness. A similar study is presented for the isolated (category 1) shear loaded plate with edges clamped on all four sides, which although is of little importance from a practical view point, provides one of the limiting cases commonly given in the literature. A selection of results for comparison with others is given in Table 4(a) for pure compression and 4(b) for pure shear loading. The close agreement, obtained for the compression loaded plate, can be seen to extend to the more complex clamped shear buckling problem.

The skew angle range for the plate results has been restricted to $0° \leqslant \alpha \leqslant 45°$ since few investigators (Durvasula, 1970; Kennedy and Prabhakara, 1978/79) have presented comparative results for skew angles outside this range. However, a test for $\alpha = 60°$ reveals a similar buckling factor correlation to others (Durvasula, 1970) in Table 4, for clamped compression loaded plates: 109.3(130.5); 38.91(42.14); 31.58(36.84) and 29.50(39.35) and clamped negative and positive shear loaded plates: −82.50, 167.0(−85.0, 531.5); −45.80, 57.35(−46.58, 69.86); −39.27, 41.54(−40.24, 45.83) and −37.54, 38.44(−39.38, 44.40), which correspond to side ratios $a/b = 0.5$, 1, 1.5 and 2, respectively.

Buckling design curves for the clamped compression loaded plate are shown in Fig. 7 and correspond to the buckling factor ($k = \sigma b^2 t/\pi^2 D$) results of Table 4(a). Here, the use of a modified buckling factor $k'(= k \cdot \cos^6 \alpha)$ achieves a compact scale and improves the nesting qualities of the curves.

Support conditions for the clamped compression results prevent in-plane displacement (u) and out-of-plane displacement and rotation w and ψ respectively, for longitudinal supports. Transverse skew boundaries consist of 23 equally spaced point supports across the plate, to which constraints u, w and $\psi_y(= \partial w/\partial x)$ are applied. Since compression and shear loads are not combined in the results that follow, the in-plane displacement (u) constraints on the transverse skew boundary edges were replaced with v constraints for the

Table 2. Stiffened benchmark panel buckling load factor results for skew angle $\alpha = 0^\circ$, giving comparisons for the three categories: (1) isolated, using EAL results from Stroud *et al.* (1984); (2) uni-axial continuity from York and Williams (1995); and (3) bi-axial continuity. Orthotropic "smeared" stiffnesses are given for each panel. Category (1) STAGS results for load case 1 are 1.5565 and 0.8179 for the composite and metal blade-stiffened panels, respectively

Panel category	Composite blade-stiffened (1) EAL	Composite blade-stiffened (2) Uni-	Composite blade-stiffened (3) Bi-	Metal blade-stiffened (1) EAL	Metal blade-stiffened (2) Uni-	Metal blade-stiffened (3) Bi-	Composite hat-stiffened (1) EAL	Composite hat-stiffened (2) Uni-	Composite hat-stiffened (3) Bi-	Metal j-stiffened (1) EAL	Metal j-stiffened (2) Uni-	Metal j-stiffened (3) Bi-
Load case 1	1.552	1.659	1.679	0.8138	0.8429	0.8437	3.192	3.281	3.285	1.042	1.116	1.117
2	—	—	—	—	—	—	—	—	—	0.948	1.014	1.015
3	1.206	1.282	1.299	0.6061	0.6307	0.6322	2.680	2.745	2.752	0.825	0.8561	0.8563
5	0.4764	0.4901	0.4913	0.1929	0.1932	0.1933	1.406	1.451	1.454	—	—	—
D_{11}		9221.1 Nm			10064 Nm			27373 Nm			20155 Nm	
D_{22}		326.88 Nm			65.31 Nm			53.98 Nm			65.31 Nm	
D_{33}		180.97 Nm			35.55 Nm			961.64 Nm			36.62 Nm	

Table 3. Percentage increase in buckling load capacity between category (2) and category (3) results for the four benchmark panels with pure shear loading over skew angle range $-60^\circ \leqslant \alpha \leqslant 60^\circ$

Panel\\α	-60°	-30°	0°	30	60
Composite blade-stiffened	0.2	1.2	1.2	7.8	8.1
Metal blade-stiffened	0.2	0.2	0.1	0.7	0.5
Composite hat-stiffened	0.2	0.4	0.1	0.6	1.2
Metal j-stiffened	0.1	0.3	0.1	0.3	0.3

clamped shear results in order to reduce solution time. Design curves for the clamped shear loaded plate are given in Fig. 8, on which the direction of positive shear loading is also illustrated along with plate geometry and boundary conditions.

As an independent check on the modelling accuracy, comparison was made with the convergence study in Anderson *et al.* (1983) for a square, shear loaded clamped plate, but with transverse boundaries ($\alpha = 0^\circ$) simply supported. This revealed that 8 equally spaced point supports and 8 terms in the deflection series (i.e. the number of m values taken from Table 1 with $\pm$ values counted as one term) were sufficient for good convergence. Their buckling coefficient $k = 13.07$, with a mode repetition over length a. The result obtained using 23 point supports and 10 terms (i.e. $q_{max} = 10$) in the deflection series gave $k = 13.08$, corresponding to the same mode repetition ($\xi = 0.1$ in Table 1).

Simple support conditions at longitudinal and transverse (skew) boundaries prevent out-of-plane (w) displacement only, with the exception of a single v displacement constraint in order to avoid any in-plane Euler modes, which may occur in the infinitely long plate. These conditions were maintained for the shear buckling case since results were virtually unaffected by the addition of in-plane u constraints at longitudinal boundaries and increasing the number of v constraints along transverse (skew) boundaries.

Buckling factor ($k' = k \cdot \cos^6 \alpha$) curves for compression loaded plates are illustrated in Fig. 9(a). These represent category (2) results, i.e. uni-axial continuity. Category (3) results are illustrated in Fig. 9(b), which demonstrates the effect of bi-axial continuity by comparison with uni-axial results reproduced from (a). Similarly, Fig. 10(a)–(d) illustrates the equivalent results for shear loading. For category (2) results, the effect of both positive and negative shear loading is demonstrated in (a) and (b) respectively. These results are superimposed on the equivalent category (3) results in (c) and (d), demonstrating the additional effect that transverse continuity has on shear loaded plates.

Results are presented in Table 5 for a range of skew angles and aspect-ratios, which demonstrate the significant percentage increases in buckling load capacity of category (2) plates resulting from the addition of transverse continuity over supports, i.e. to become category (3).

Details of the mode interaction between skew angle and aspect-ratio for the plate results are tabulated in Appendix 1. They list the more usual form of buckling factor $k(= \sigma b^2 t/\pi^2 D)$ results and complement the curves of Figs 7–10, to which they correspond.

4. CONCLUDING REMARKS

A comprehensive study of the buckling characteristics of compression and shear loaded skew plates and plate assemblies has been presented. A classification system is proposed by which these structures may be categorised with respect to their continuity over supports, and comparison of these categories has revealed, through the buckling results obtained herein, the potential limitations of modelling an isolated plate assembly, as is often done in practice, for which the real problem has continuity over supports in either one or both in-plane directions, e.g. as in aircraft wing or fuselage construction.

Stiffened panel results suggest that a design would be virtually unaltered if transverse continuity effects were ignored for panels of this type, but significant effects result from

Table 4. Category (1), clamped plate buckling factor comparisons for (a) pure compression loading ($k = \sigma_x b^2 t/\pi^2 D$) and (b) pure shear loading ($k = \sigma_{xy} b^2 t/\pi^2 D$) with varying aspect-ratio and skew angle α

(a)

a/b	0.5				1				1.5				2			
α	0°	15°	30°	45°	0°	15°	30°	45°	0°	15°	30°	45°	0°	15°	30°	45°
Guest (1951)							13.53	20.72								
Wittrick (1953)							13.64	21.64								
Argyris (1966)					10.15	—	13.76	20.44	8.39	—	12.32	17.99				
Durvasula (1970)	19.35	21.63	30.38	55.26	10.08	10.87	13.58	20.44	—	8.97	11.16	17.10	8.03	8.70	10.53	15.74
Author	19.34	21.63	30.58	54.65	10.07	10.85	13.58	20.21	8.35	8.96	11.06	16.30	7.87	8.41	10.31	15.18

(b)

a/b	0.5				1				1.5				2			
α	0°	15°	30°	45°	0°	15°	30°	45°	0°	15°	30°	45°	0°	15°	30°	45°
Wittrick (1954)								−24.32								
Argyris (1966)					±14.88	—	−16.69	−24.41	±11.67	—	−14.12	−20.64				
Durvasula (1970)	—	−34.58	−31.58	−40.54	—	−14.39	−16.66	−24.08	—	−12.01	−14.05	−20.21	—	−10.84	−13.34	−19.24
		55.36	76.90	128.3		17.24	23.64	32.56		12.73	15.19	22.37		11.10	13.73	20.35
Fried and Schmitt (1972)					±14.53	−10.93	−9.36	−9.25	±11.42	−8.74	−7.42	−7.29	±10.21	−7.75	−6.76	−6.75
						22.13	39.64	88.73		17.13	30.26	66.98		15.48	27.58	61.31
Author	±41.09	−34.83	−31.48	−40.44	±14.70	−14.41	−16.63	−24.04	±11.50	−12.05	−14.03	−20.18	±10.26	−10.84	−13.31	−19.19
		48.63	62.99	92.76		17.18	22.17	31.65		12.29	15.10	21.91		11.09	13.62	19.86

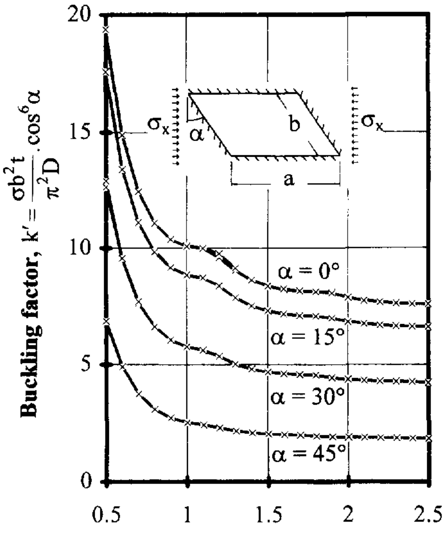

Fig. 7. Category (1) buckling factor curves ($k' = k.\cos^6\alpha$) for clamped compression loaded skew plate.

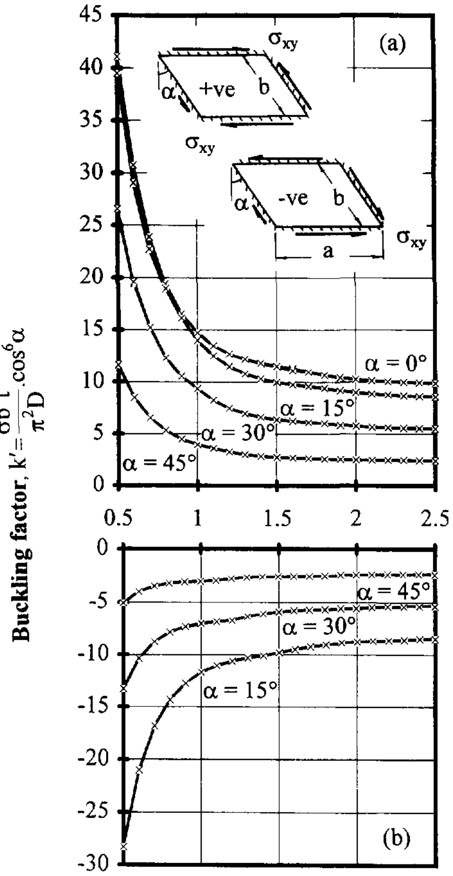

Fig. 8. Category (1) buckling factor curves ($k' = k.\cos^6\alpha$) for clamped (a) positive and (b) negative shear loaded skew plate. (Note that the positive shear direction is opposite to that of the stiffened panel results.)

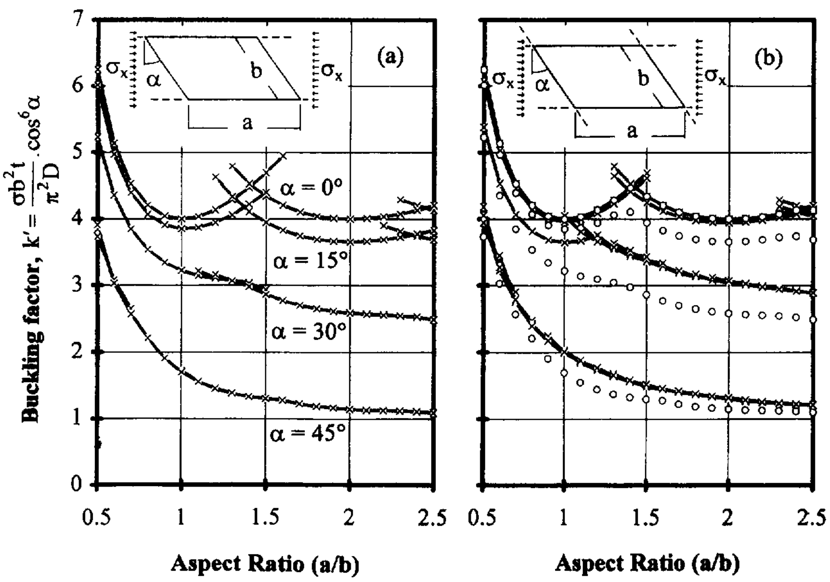

Fig. 9. Buckling factor curves ($k' = k.\cos^6\alpha$) for (a) category (2) and (b) category (3) simply supported compression loaded skew plate. Discrete results from (a) are superimposed (o) for comparison on (b).

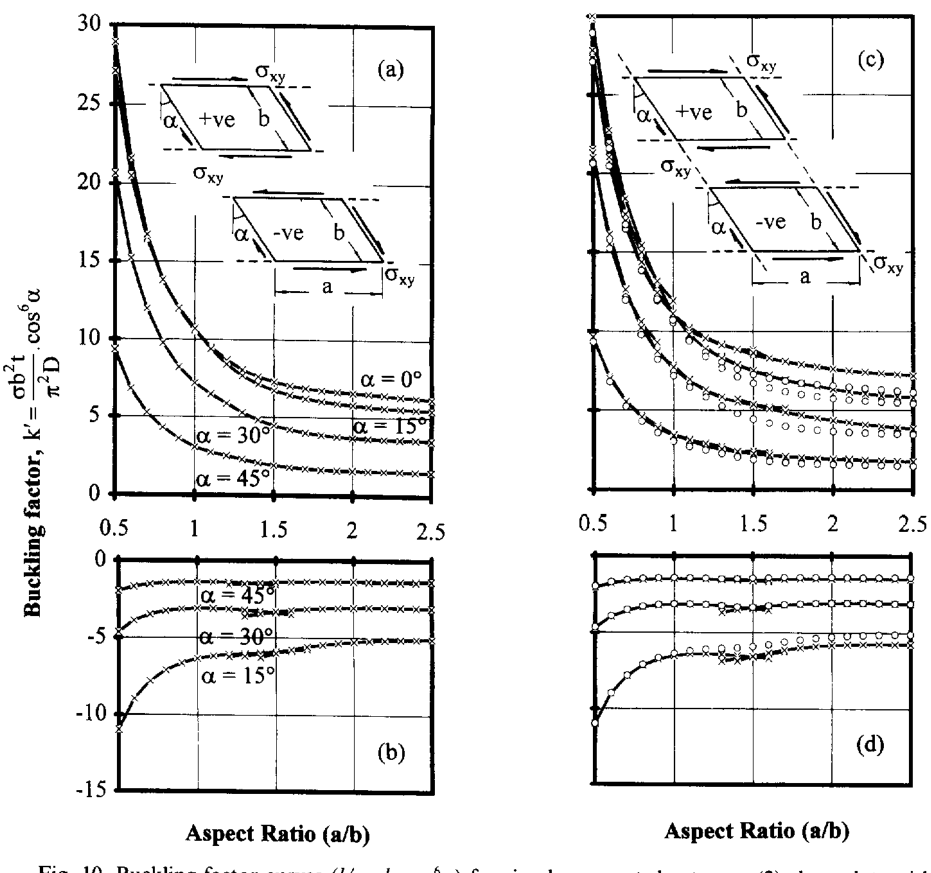

Fig. 10. Buckling factor curves ($k' = k.\cos^6\alpha$) for simply supported category (2) skew plate with (a) positive shear load and (b) negative shear load. Equivalent category (3) results are given for (c) positive and (d) negative shear load with discrete results from (a) and (b) superimposed (o) for comparison. (Note that the positive shear direction is opposite to that of the stiffened panel results.)

Table 5. Percentage increase in buckling load capacity between category (2) and category (3) plate results for shear and compression loading with varying aspect-ratio and skew angle α

a/b	0.5				1				1.5				2			
Loading\\α	0°	15°	30°	45°	0°	15°	30°	45°	0°	15°	30°	45°	0°	15°	30°	45°
Compression	0	0.8	2.9	5.7	0	2.9	13.4	17.3	0	7.5	17.3	14.7	0	7.9	17.8	13.8
Positive shear	2.1	3.1	1.8	1.6	4.9	3.8	5.7	11.8	16.9	11.1	20.5	18.7	16.0	10.1	18.8	21.3
Negative shear	2.1	0.1	1.4	4.1	4.9	2.5	1.0	6.2	16.9	10.6	0.9	11.1	16.0	10.5	0.5	7.8

continuity parallel to the direction in which the stiffeners run. This point is seen to be especially true for loading cases with a high compression component, which is demonstrated by comparison with accurate results of the finite element codes EAL and STAGS for the equivalent isolated rectangular panel. Isotropic plate results on the other hand, show an equally marked effect on the load carrying capacity when the plate is continuous transversely, both for compression and shear buckling problems, since these results are free from the orthotropic influence of stiffeners.

The skew angle range for the plate results has been restricted to $0^\circ \leqslant \alpha \leqslant 45^\circ$ since this accords with comparative results presented by the majority of investigators. However, tests have revealed a similarly close correlation for results above $\alpha = 45^\circ$.

Finally, clamped plate results give good agreement with other published results for compression loading by virtue of the boundary conditions which, by implication, degenerate into isolated plates and furthermore, this agreement extends to the more complex clamped shear buckling problem.

Acknowledgements—The work flows partially from a Ph.D. thesis by the author, under the supervision of Professor F. W. Williams, with financial support from the Science and Engineering Research Council and sponsorship from NASA under Co-operative Agreement No. NCCW-000002, BAe Defence Military Aircraft (Warton) and BAe Airbus Ltd. The author is currently supported by the Engineering and Physical Sciences Research Council, grant No. GR/J79430.

REFERENCES

Anderson, M. S., Williams, F. W. and Wright, C. J. (1983). Buckling and vibration of any prismatic assembly of shear and compression loaded anisotropic plates with an arbitrary supporting structure. *Int. J. Mech. Sci.* **25**, 585–596.

Anderson, R. A. (1951). Charts giving critical compressive stress of continuous flat sheet divided into parallelogram-shaped panels. *TN* 2392, National committee for Aeronautics (NACA), Washington, D.C.

Argyris, J. H. (1966). Continua and discontinua (an apercu of recent developments of the matrix displacement method). In *Matrix Methods in Structural Mechanics*, pp. 11–190. (Proceedings of the conference held at Wright-Patterson Air Force Base, Ohio, Oct. 26-28, 1965.)

Bushnell, D. (1987). PANDA2—program for minimum weight design of stiffened, composite, locally buckled panels. *Comput. Struct.* **25**, 469–605.

Durvasula, S. (1970). Buckling of clamped skew plates. *AIAA J.* **8**, 178–181.

Durvasula, S. (1971). Buckling of simply supported skew plates. *J. Engng Mech. Div., ASCE* **97**, 967–979.

Fried, I. and Schmitt, K. H. (1972). Numerical results from the application of gradient iterative techniques to the finite element vibration and stability analysis of skew plates. *Aeronaut. J.* **76**, 166–169.

Guest, J. (1951). The buckling of uniformly compressed parallelogram plates having all four edges clamped. SM 172, Aeronaut. Res. Labs, Melbourne, Australia.

Jones, R. M. (1975). *Mechanics of Composite Materials*, McGraw-Hill, New York.

Kennedy, J. B. and Prabhakara, M. K. (1978). Buckling of simply supported orthotropic skew plates. *Aeronaut. Q.* **29**, 161–174.

Kennedy, J. B. and Prabhakara, M. K. (1979). Combined-load buckling of orthotropic skew plates. *J. Engng Mech. Div., ASCE* **105**, 71–79.

Mizusawa, T., Kajita, T. and Naruoka, M. (1980). Analysis of skew plate problems with various constraints. *J. Sound Vib.* **73**, 575–584.

Mizusawa, T. and Kajita, T. (1986). Vibration and buckling of skew plates with edges elastically restrained against rotation. *Comput. Struct.* **22**, 987–994.

Morley, L. S. D. (1963). *Skew Plates and Structures*. Pergamon Press, Oxford.

Peshkam, V. and Dawe, D. J. (1989). Buckling and vibration of finite-length composite prismatic plate structures with diaphragm ends, part II: computer programs and buckling applications. *Comp. Meth. Appl. Mech. Engng* **77**, 227–252.

Prabhu, M. S. S. and Durvasula, S. (1972). Stability of clamped skew plates. *Appl. Sci. Res.* **26**, 255–271.

Stroud, W. J., Greene, W. H. and Anderson, M. S. (1984). Buckling loads of stiffened panels subjected to combined longitudinal compression and shear: results obtained with PASCO, EAL, and STAGS computer programs. NASA Technical paper 2215.

Thangam Babu, P. V. and Reddy, D. V. (1978). Stability analysis of skew orthotropic plates by the finite strip method. *Comput. Struct.* **8**, 599–607.

Wang, C. M., Liew, K. M. and Alwis, W. A. (1992). Buckling of skew plates and corner condition for simply supported edges. *J. Engng Mech., ASCE* **118**, 651–662.

Williams, F. W. and Anderson, M. S. (1983). Incorporation of Lagrangian multipliers into an algorithm for finding exact natural frequencies or critical buckling loads. *Int. J. Mech. Sci.* **25**, 579–584.

Williams, F. W. and Anderson, M. S. (1985). Buckling and vibration analysis of shear-loaded prismatic plate assemblies with supporting structures, utilizing symmetric or repetitive cross-sections. In *Aspects of the Analysis of Plate Structures*—a volume in honour of W. H. Wittrick (ed. Dawe, D. J., Horsington, R. W., Kamtekar, A. G. and Little, G. H.), pp. 51–71. Oxford University Press, Oxford.

Williams, F. W., Kennedy, D., Butler, R. and Anderson, M. S. (1991). VICONOPT: program for exact vibration and buckling analysis or design of prismatic plate assemblies. *AIAA J.* **29**, 1927–1928.

Wittrick, W. H. (1953). Buckling of oblique plates with clamped edges under uniform compression. *Aeronaut. Q.* **4,** 151–163.
Wittrick, W. H. (1954). Buckling of oblique plates with clamped edges under uniform shear. *Aeronaut. Q.* **5,** 39–51.
Wittrick, W. H. (1956). On the buckling of oblique plates in shear. *Aircraft Engng* **28,** 25–27.
Wittrick, W. H. and Williams, F. W. (1973). An algorithm for computing critical buckling loads of elastic structures. *J. Struct. Mech.* **1,** 497–518.
Wittrick, W. H. and Williams, F. W. (1974). Buckling and vibration of anisotropic or isotropic plate assemblies under combined loadings. *Int. J. Mech. Sci.* **16,** 209–239.
York, C. B. (1993). Buckling of prismatic and skewed repetitive aerospace panels. Ph.D. thesis, University of Wales.
York, C. B. and Williams, F. W. (1994). Theory and buckling results for infinitely wide, stiffened skew plate assemblies. *Comput. Struct.* **28,** 189–200.
York, C. B. and Williams, F. W. (1995). Buckling analysis of skew plate assemblies: classical plate theory results incorporating Lagrangian multipliers. *Comput. Struct.* **56,** 625–635.

APPENDIX

This section presents tabulated buckling factor results for skew plates, which correspond to the design curves of Figs 7–10. For each table, underlined results are the critical buckling factors ($k = \sigma b^2 t/\pi^2 D$) and adjacent results give the necessary cusp information from which the buckling envelope for each skew angle is then drawn. The ξ value corresponds to the specific combination of longitudinal half-wavelengths in Table 1 which caused buckling and for bi-axial continuity results, the g relates to the corresponding transverse half-wavelength in eqns (17) and (18), with $P = 1$.

Table A1. Category (1) clamped buckling factor ($k = \sigma_x b^2 t/\pi^2 D$) results for skew plate with pure compression loading, cf. Fig. 7. Highlighted results for a/b = 1 were given in York and Williams (1995)

α	a/b / ξ	0.5	0.6	0.7	0.8	0.9	1.0	1.1	1.2	1.3	1.4	1.5	1.6	1.7	1.8	1.9	2.0	2.1	2.2	2.3	2.4	2.5
0°	1						10.109	9.994	9.581	8.999	8.605	8.351	8.201	8.127	8.103	8.099						
	0.9												8.231	8.141	8.103	8.049	7.873					
	0.1					10.386	10.075	9.989	9.743	9.120									7.658	7.607	7.582	7.574
	0	19.339	14.889	12.444	11.090	10.384	10.074	9.989	9.767					8.144	8.106	8.042	7.867	7.742	7.657	7.607	7.582	7.574
15°	1					11.278	10.853	10.703	10.278										8.203	8.149	8.123	8.115
	0.9				12.164	11.274	10.853	10.704	10.278	9.653	9.230	8.959	8.799	8.718				8.294	8.203	8.149	8.123	8.115
	0.8										9.232	8.959	8.799	8.718	8.686							
	0.1	21.634	16.514	13.685	12.104	11.260	10.864	10.717				8.973	8.800	8.713	8.681	8.583	8.407	8.282	8.199	8.150	8.127	
	0												8.802	8.713	8.681	8.586	8.410					
30°	0.9	29.950	22.638	18.179	15.659	14.278	13.581	13.264	12.683			11.077	10.895	10.803	10.735	10.486	10.311	10.197	10.132	10.136	10.086	
	0.2																		10.135	10.099	10.078	9.973
	0.1	30.578	22.659	18.235		14.318	13.593	13.244	12.661	11.886	11.376	11.061	10.888	10.807	10.747			10.205	10.136	10.099	10.079	9.972
45°	0.9	54.647	39.203	30.038	24.775		20.248	19.425	18.400	17.334	16.674	16.303	16.111	15.899	15.551		15.188	15.115	15.021	14.870	14.767	14.707
	0.1	54.729	39.266	30.032	24.735	21.775	20.207	19.401	18.404	17.344		16.315	16.119	15.897	15.545	15.315	15.181	15.111	15.023	14.873		

Table A2. Category (1) clamped buckling factor ($k = \sigma_{xy}b^2t/\pi^2D$) results for skew plate with pure positive shear loading, cf. Fig. 8(a)

α	ξ \ a/b	0.5	0.6	0.7	0.8	0.9	1	1.1	1.2	1.3	1.4	1.5	1.6	1.7	1.8	1.9	2	2.1	2.2	2.3	2.4	2.5
0°	1	41.093	30.743	23.894	19.398	16.543	14.696	13.484	12.678	12.137	11.768											
	0.9							13.485	12.679	12.137	11.766	11.504	11.304									
	0.7																			9.979	9.917	9.864
	0.6																		10.054	9.977	9.916	9.865
	0.4									12.178	11.781	11.494	11.271	10.989								
	0.2										11.790	11.495	11.267	10.975	10.671							
	0.1											11.495	11.085	10.971	10.667	10.435	10.261	10.132	10.039	9.971	9.921	9.880
15°	1																			10.674	10.597	10.540
	0.9	48.634	35.720	27.889	23.346	19.852	17.175	15.360	14.136	13.308							11.097	10.914	10.776	10.673	10.597	10.540
	0.8		35.812	27.952	23.345	19.861	17.182									11.331	11.067	10.914	10.778	10.677		
	0.1						17.242	15.381	14.124	13.272	12.691	12.291	12.011	11.805	11.606	11.313	11.088	10.916	10.788			
30°	1													14.481	14.269	13.907	13.624	13.413	13.260	13.150	13.073	13.013
	0.9																		13.260	13.150	13.071	13.010
	0.7												14.748	14.476	14.262	13.913	13.629					
	0.6																			13.154	13.073	13.011
	0.5	62.993	46.012	36.032																		
	0.4	63.018	45.999	36.014	29.174	25.019																
	0.1		46.429	36.052	29.135	24.972	22.173	19.542	17.715	16.479	15.654	15.104	14.733	14.473	14.274	13.933						
45°	0.9						31.690	28.637	25.805	23.906	22.684	21.911	21.416	21.076	20.614	20.176				19.399	19.272	19.108
	0.8												21.417	21.077	20.614	20.175	19.865					
	0.4					35.862	31.661	28.631	25.810	23.915												
	0.3	92.760	68.030	52.400																		
	0.1	92.842	67.914	52.325	42.761	35.827	31.650	28.633	25.813					21.084	20.615	20.173	19.860	19.645	19.498	19.395	19.271	19.109

Table A3. Category (1) clamped buckling factor ($k = \sigma_{xy} b^2 t / \pi^2 D$) results for skew plate with pure negative shear loading, cf. Fig. 8(b)

α	a/b ξ, g	0.5	0.6	0.7	0.8	0.9	1	1.1	1.2	1.3	1.4	1.5	1.6	1.7	1.8	1.9	2	2.1	2.2	2.3	2.4	2.5
15°	1				17.615	15.655	14.406	13.600	13.074	12.723	12.472	12.049										
	0.9		25.931	20.736	17.606	15.652	14.406	13.602		12.724	12.471	12.047	11.653	11.360	11.144							
	0.8								13.084	12.730	12.470	12.048	11.654									
	0.5											12.063	11.660	11.356	11.133	10.970						
	0.4																			10.638	10.531	10.435
	0.3																	10.759	10.697	10.637	10.529	10.435
	0.2	34.842	25.830	20.713	17.638	15.722																
	0.1	34.831	25.825	20.713	17.642								11.675	11.358	11.125	10.956	10.836	10.753	10.694	10.641	10.529	10.436
	0															10.957	10.836	10.752	10.694	10.647	10.532	
30°	1					17.480	16.679	16.206	15.910	15.053	14.449	14.032	13.753	13.573	13.463	13.397	13.350					
	0.9						16.673	16.206	15.908	15.058	14.453											
	0.3													13.602	13.473	13.393	13.324	13.126				
	0.1			20.811	18.618	17.352	16.629	16.213	15.942										12.966	12.859	12.786	12.739
	0	31.478	24.619	20.805	18.615	17.352	16.633								13.481	13.396	13.307	13.112	12.965	12.859	12.786	12.740
45°	0.9					24.416	24.063	23.077	21.756	20.923	20.433	20.177	20.073	20.044	19.679				19.050	19.033	18.894	18.771
	0.2											20.201	20.083	20.044	19.644	19.365						
	0.1	40.442	31.978	27.544	25.321	24.353	24.042	23.200	21.845				20.084	20.044	19.641	19.363	19.185	19.087	19.043	19.031	18.914	18.786

Table A4. Category (2) simply supported buckling factor ($k = \sigma_x b^2 t/\pi^2 D$) results for skew plate with pure compression loading, cf. Fig. 9(a). Highlighted results for $a/b = 1$ were given in York and Williams (1995)

α	ξ \ a/b	0.5	0.6	0.7	0.8	0.9	1.0	1.1	1.2	1.3	1.4	1.5	1.6	1.7	1.8	1.9	2.0	2.1	2.2	2.3	2.4	2.5
0°	1	6.250	5.138	4.531	4.202	4.045	4.000	4.036	4.134	4.282	4.470	4.694	4.951							4.289	4.202	4.134
	0									4.789	4.531	4.340	4.202	4.107	4.045	4.011	4.000	4.010	4.036	4.079	4.134	4.202
15°	1	7.410	6.119	5.406	5.012	4.813	4.743	4.765	4.856	5.002	5.193	5.415							4.804	4.698	4.612	4.546
	0								5.699	5.337	5.061	4.861	4.716	4.615	4.550	4.515	4.504	4.515	4.544	4.588	4.653	4.717
30°	1	12.394	10.319	9.121	8.389	7.928	7.634	7.452	7.343	7.271									6.078	6.021	5.975	5.903
	0.9						7.645	7.456	7.343	7.274	7.216							6.109	6.053	6.021	5.978	5.905
	0.5																6.146	6.086	6.048	6.025	6.009	
	0.4							7.627	7.383	7.244	7.173	6.952										
	0.1														6.277	6.185	6.121	6.078	6.050	6.031		
	0							7.494	7.271	7.051	6.778	6.564	6.399	6.275	6.185	6.121	6.079					
45°	1							12.382	11.553	10.984	10.624	10.397	10.199	9.809								
	0.9						13.740	12.427	11.551	10.984	10.627	10.400	10.198	9.807	9.519	9.312	9.169					
	0.6	29.898	24.684	21.184																		
	0.5													9.821	9.525	9.311	9.162	9.063				
	0.2	30.765	24.234	20.599	17.708																	
	0.1				17.668	15.241	13.543	12.376	11.597	11.095					9.533	9.311	9.156	9.051	8.983	8.939	8.871	8.762
	0	31.300	24.249	20.532	17.661	15.239	13.546	12.382										9.053	8.984	8.938	8.874	8.765

Table A5. Category (3) simply supported buckling factor ($k = \sigma_x b^2 t/\pi^2 D$) results for skew plate with pure compression loading, cf. Fig. 9(b). Anderson (1951) gave results of 6.74 and 11.46 corresponding to $\alpha = 30°$ and 45° respectively, with $a/b = 1$

α	a/b / ξ, g	0.5	0.6	0.7	0.8	0.9	1.0	1.1	1.2	1.3	1.4	1.5	1.6	1.7	1.8	1.9	2.0	2.1	2.2	2.3	2.4	2.5
0°	1,1	6.250	5.138	4.531	4.202	4.045	4.000	4.036	4.134	4.282	4.470	4.694								4.289	4.202	4.134
	0,1									4.789	4.531	4.340	4.202	4.107	4.045	4.011	4.000	4.010	4.036	4.079	4.134	4.202
15°	1,1	7.469	6.191	5.493	5.115	4.933	4.882	4.924	5.037	5.206	5.423	5.680								5.152	5.059	4.987
	1,2									5.719	5.435	5.224	5.073	4.969	4.903	4.868	4.859	4.872	4.906	4.956	5.022	5.103
30°	1,1	12.759	10.752	9.649	9.043	8.744	8.654	8.716	8.891													
	1,2										8.328	7.988	7.758	7.557	7.423	7.337	7.283					
	0.8,2									8.624	8.328	7.951	7.806	7.595								
	0.7,2													7.639	7.444	7.314	7.234	7.186				
	0.6,2								8.919	8.452	8.165	8.003	7.916									
	0.5,2														7.515	7.304	7.213	7.138	7.094			
	0.4,2							9.258	8.732	8.415	8.238	8.142										
	0.3,2															7.407	7.239	7.124	7.053	7.011		
	0.2,2						9.615	9.036	8.687	8.490	8.379						7.269	7.134	7.045	6.994	6.909	6.844
	0,2																	7.168	7.052	6.975	6.899	6.846
45°	1,2									13.457	12.547	11.922	11.520	11.285	11.068							
	0.8,2								14.182	13.188	12.475	12.151	11.580	11.227	10.951	10.748						
	0.7,2												11.654	11.248	10.925	10.691	10.521					
	0.6,2							15.004	13.873	13.089	12.554	12.163										
	0.5,2	31.588	26.424	23.227			16.289	14.832	13.823	13.141	12.675			11.385	10.973	10.693	10.430	10.265				
	0.4,2					17.928	16.058	14.740	13.854	13.260					11.039	10.686	10.420	10.228	10.085			
	0.3,2	32.451	25.850	22.108	19.761										10.738	10.436	10.083	10.046	9.905	9.748	9.611	
	0.2,2	33.453	26.203	21.957	19.386	17.426	15.882	14.843	14.139													
	0.1,2			22.086	19.194	17.345	15.968	15.009									10.536	10.241	10.015	9.850	9.730	9.637
	0,2		27.646	22.300	19.144	17.388	16.084											10.266	10.015	9.843	9.734	9.671

Table A6. Category (2) simply supported buckling factor ($k = \sigma_{xy} b^2 t / \pi^2 D$) results for skew plate with pure positive shear loading, cf. Fig. 10(a)

α	a/b / ξ	0.5	0.6	0.7	0.8	0.9	1.0	1.1	1.2	1.3	1.4	1.5	1.6	1.7	1.8	1.9	2.0	2.1	2.2	2.3	2.4	2.5
0°	0.7																			6.339	6.248	6.160
	0.6																		6.418	6.331	6.245	6.161
	0.5	27.118	20.556	16.581													6.591	6.498	6.413	6.330	6.247	6.167
	0.4	27.130	20.475	16.462	13.824	11.962	10.589									6.678	6.579	6.494	6.416	6.337		
	0.3			16.562	13.856	11.952	10.552	9.508	8.726													
	0.2					12.029	10.571	9.492	8.693	8.099					6.755	6.652	6.573	6.509	6.447			
	0						10.641	9.503	8.677	8.071	7.624	7.293	7.049	6.870	6.740	6.646	6.578	6.528				
15°	1															7.253	7.099	6.981	6.891	6.820	6.764	6.694
	0.9														7.453	7.252	7.099	6.982	6.892			
	0.5													7.663	7.425	7.245	7.108	7.004				
	0.2												7.923	7.634	7.417	7.253	7.129					
	0.1											8.294	7.915	7.631	7.417	7.256						
	0	35.624	26.596	20.618	17.040	14.802	13.189	11.569	10.362	9.463	8.793	8.291	7.915	7.632	7.419							
30°	1								14.003	12.505	11.380	10.542	9.921	9.462	9.124	8.876	8.695	8.565	8.470	8.400	8.346	8.274
	0.8							15.476	13.941	12.502	11.386	10.551										
	0.6						17.130	15.360	13.891	12.516	11.414											
	0.5					19.565	17.084	15.346	13.900	12.537										8.425	8.359	8.260
	0.4	49.046	36.127	28.373	23.156	19.516	17.074	15.368	13.937													
	0.3	48.907	36.079	28.409	23.169																	
45°	1	74.999	54.508	41.968	34.409	28.743	24.406	21.724	20.006	18.316	16.549											
	0.9							21.732	20.013	18.315	16.546	15.252	14.326	13.674	13.220	12.909	12.697	12.553	12.451			
	0.8	74.593	54.622	42.167																		
	0.1															12.924	12.702	12.550	12.443	12.340	12.097	11.906

Table A7. Category (2) simply supported buckling factor ($k = \sigma_{xy} b^2 t/\pi^2 D$) results for plate with pure negative shear loading, cf. Fig. 10(b)

α	a/b / ξ	0.5	0.6	0.7	0.8	0.9	1.0	1.1	1.2	1.3	1.4	1.5	1.6	1.7	1.8	1.9	2.0	2.1	2.2	2.3	2.4	2.5
15°	1	13.517	11.026	9.587	8.711	8.164	7.823	7.609	7.485	7.417	7.385	7.369										
	0.6								7.682	7.488	7.364	7.289	7.245									
	0.4									7.625	7.412	7.265	7.162	7.080								
	0										7.747	7.388	7.107	6.887	6.715	6.582	6.480	6.404	6.349	6.310	6.285	6.270
30°	1	10.992	9.259	8.304	7.777	7.507	7.404	7.415	7.506	7.656	7.851	8.078	8.330									
	0									8.622	8.210	7.901	7.671	7.504	7.387	7.309	7.264	7.247	7.252	7.277	7.318	7.373
45°	1	15.835	13.555	12.300	11.618	11.290	11.200	11.283	11.492	11.798	12.177	12.614						11.492	11.297	11.145	11.031	10.950
	0								12.721	12.133	11.702	11.394	11.181	11.046	10.974	10.954	10.976	11.034	11.123	11.237	11.370	

Table A8. Category (3) simply supported buckling factor ($k = \sigma_{xy}b^2t/\pi^2D$) results for skew plate with pure positive shear loading, cf. Fig. 10(c)

α	a/b ξ, g	0.5	0.6	0.7	0.8	0.9	1.0	1.1	1.2	1.3	1.4	1.5	1.6	1.7	1.8	1.9	2.0	2.1	2.2	2.3	2.4	2.5
0°	1,2															7.802	7.634	7.506	7.410	7.339	7.285	7.246
	0.8,2														7.937	7.761	7.623	7.514	7.425			
	0.7,2													8.116	7.911	7.751	7.627	7.528	7.442	7.360	7.279	7.222
	0.6,2												8.326	8.085	7.899	7.755	7.642			7.378	7.294	7.219
	0.5,2	27.694	20.774	16.801								8.579	8.292	8.073	7.904	7.772						
	0.4,2	27.842	20.724	16.612	14.100	12.480					8.882	8.540	8.279	8.080	7.925							
	0.3,2		21.020	16.689	14.036	12.335	11.191			9.240	8.837	8.527	8.289	8.106								
	0.2,2			16.979	14.139	12.314	11.098	10.256	9.645	9.181	8.821	8.840	8.324									
	0.1,2				14.369	12.386	11.074	10.189	9.580													
	0,2					12.454	11.078	9.979	9.558	9.143	8.856	8.651										
15°	1,2															8.068	7.819	7.620	7.466	7.347	7.257	7.186
	0.9,2														8.292	8.041	7.818	7.625	7.471	7.350	7.257	7.183
	0.8,2													8.561	8.264	8.026	7.823	7.642				
	0.7,2												8.886	8.529	8.250	8.028	7.841			7.374	7.264	7.176
	0.6,2											9.282	8.848	8.515	8.256	8.049						
	0.5,2										9.770	9.234	8.831	8.523	8.282							
	0.4,2									10.380	9.708	9.213	8.840	8.555								
	0.2,2								11.060	10.250	9.671	9.249	8.929									
	0.1,1		26.956	21.515	18.338	16.192	14.683															
	0,2	36.719	28.017	22.656	18.988	16.063	13.692	12.076	10.978	10.222	9.691	9.307										
	0,1	36.942	26.849	21.429	18.458	16.244																
30°	1,2														11.064	10.658	10.328	10.016	9.704	9.456	9.258	9.100
	1,1						18.700	16.309	14.752	13.752	13.112	12.700	12.428	12.232								
	0.9,2													11.556	11.059	10.657	10.329	10.024				
	0.8,2												12.140	11.538	11.053	10.662	10.342			9.473	9.263	9.095
	0.7,2											12.833	12.105	11.523	11.057	10.681						
	0.7,1					20.903	18.108	16.225	14.889	13.910												
	0.6,1				24.738	20.682	18.040	16.275	15.002													
	0.5,2	51.020	37.035	29.358	24.988	22.087					13.604	12.748	12.076	11.546	11.123							
	0.4,2	50.483	36.756	29.434	25.152																	
	0.4,1	49.799	38.109	30.096	24.278	20.553	18.179	16.552														
	0.3,1		38.219	29.986	24.248	20.676	18.383															
45°	1,2			44.880	36.144	30.651	27.622	25.507														
	1,1	77.090	56.223	44.372	37.543	32.144	27.932	24.798	22.038	20.225	19.057	18.283								14.621	14.410	14.213
	0.9,2	75.778	57.280	44.776																		
	0.9,1	76.985	55.996	44.410	37.510														14.880	14.613	14.409	14.216
	0.8,2								23.425	21.863	19.044	19.609	18.899									
	0.8,1					32.086	27.803	24.639	22.166	20.307								15.188	14.856	14.606	14.418	14.225
	0.7,2				36.541	30.966	27.297	25.000	23.299													
	0.6,1									20.553	19.109	18.108	17.419	16.925			15.501	15.117	14.833	14.625	14.466	
	0.4,1										19.310	18.152	17.339	16.771	16.358	15.864	15.420	15.536	14.862	14.687		
	0.2,1											18.306	17.378	16.716	16.242	15.776	15.400	15.133	14.936			
	0,1												17.445	16.731	16.216	15.752	15.418	15.182				

Table A9. Category (3) simply supported buckling factor ($k = \sigma_{xy} b^2 t / \pi^2 D$) results for skew plate with pure negative shear loading, cf. Fig. 10(d)

α	a/b / ξ, g	0.5	0.6	0.7	0.8	0.9	1.0	1.1	1.2	1.3	1.4	1.5	1.6	1.7	1.8	1.9	2.0	2.1	2.2	2.3	2.4	2.5
15°	1, 1	13.533	11.054	9.637	8.796	8.299	8.021	7.890	7.861	7.902	7.989	8.102	8.217									
	0.3, 1									8.457	8.218	8.038	7.874	7.702								
	0, 1										8.438	8.055	7.762	7.538	7.370	7.248	7.162	7.107	7.077	7.067	7.074	7.094
30°	1, 1	11.141	9.408	8.444	7.898	7.606	7.480	7.470	7.547	7.690	7.884	8.121	8.390									
	0, 1									8.713	8.292	7.974	7.736	7.560	7.435	7.352	7.302	7.281	7.285	7.309	7.352	7.410
45°	1, 1	16.489	14.274	13.059	12.383	12.029	11.889	11.901	12.030	12.249	12.541	12.895	13.300									
	0, 1									11.990	11.891	12.657	12.360	12.142	11.990	11.891	11.836	11.821	11.838	11.884	11.956	12.050